



# Numerical simulations on the temperature gradient and thermal stress of a thermoelectric power generator



Yongjia Wu<sup>a</sup>, Tingzhen Ming<sup>a,b,\*</sup>, Xiaohua Li<sup>b</sup>, Tao Pan<sup>a</sup>, Keyuan Peng<sup>a</sup>, Xiaobing Luo<sup>a</sup>

<sup>a</sup> School of Energy and Power Engineering, Huazhong University of Science and Technology, Wuhan 430074, China

<sup>b</sup> Department of Mechanical and Energy Engineering, University of North Texas, Denton, TX 76207, USA

## ARTICLE INFO

### Article history:

Received 29 January 2014

Accepted 16 August 2014

Available online 29 September 2014

### Keywords:

Thermoelectric power generation

Efficiency

Power output

Structure design

Thermal stress

## ABSTRACT

Thermoelectric generator is a device taking advantage of the temperature difference in thermoelectric material to generate electric power, where the higher the temperature difference of the hot-cold ends, the higher the efficiency will be. However, higher temperature or higher heat flux upon the hot end will cause strong thermal stress which will negatively influence the lifecycle of the thermoelectric module. This phenomenon is very common in industrial applications but seldom has research work been reported. In this paper, numerical analysis on the thermodynamics and thermal stress performance of the thermoelectric module has been performed, considering the variation on the thickness of materials; the influence of high heat flux on thermal efficiency, power output, and thermal stress has been examined. It is found that under high heat flux imposing upon the hot end, the thermal stress is so strong that it has a decisive effect on the life expectation of the device. To improve the module's working condition, different geometrical configurations are tested and the optimum sizes are achieved. Besides, the side effects on the efficiency, power output, and open circuit voltage output of the thermoelectric module are taken into consideration.

© 2014 Elsevier Ltd. All rights reserved.

## 1. Introduction

The thermoelectric phenomenon was first discovered as early as the 19th century. But further research on this phenomenon was not performed until the middle of the 20th when semiconductor materials with the Seebeck coefficient much higher than that of alloys were found. A basic unit of a thermoelectric power generator (TEG) is a thermocouple consisting of an n-type and a p-type thermoelectric element connected electrically in series by a conducting strip (usually copper). A typical thermoelectric device is constructed by these building-blocks connected electrically in series but thermally in parallel and sandwiched between two ceramic plates. The efficiency of the module highly depends on the temperature difference between the hot and cold end. Especially, as for the nearly 30 years, people have increasingly recognized un-sustainability and pollution of traditional energy sources, it makes much sense to have a better understanding of thermoelectric modules.

In the past three decades, the research work related to thermoelectrics has aroused much attention worldwide. The research

group led by Sahin and Yilbas [1] investigated the influence of thermoelectric pin geometry on the module's efficiency and maximum power output. They showed that the pin geometry had obvious effect on the modules with various temperature difference applied on the two ends. The feasibility to use thermoelectric generators (TEG) to power a thermoelectric cooling device (TEC) was explored by Khat tab and Shenawy [2]. They finally obtained a best match number of TEC and TEG and achieved the desired result using a solar thermoelectric generator to drive a small thermoelectric cooler in most times of the year. Thermodynamics and thermal stress analysis of a thermoelectric power generator with different pin geometry configurations was carried out by Merbati et al. [3] who managed to get the temperature and thermal stress field, and to test the thermal efficiency, maximum power output, and thermal stress in the modules. Their findings showed that the trapezoidal pins could alleviate thermal stress in the module and increase the efficiency at the same time. Rosado [14] gave a detailed description of a thermoelectric module. He especially advanced a mathematical method to estimate Thomson coefficient. A calculation model designed by Rodríguez et al. [4] was applied to examine the thermal and electrical properties of a thermoelectric module. Using the least boundary conditions, they managed to obtain a design method with better encapsulation characteristics. The research group led by O'Brien et al. [5] reviewed radioisotope

\* Corresponding author at: School of Energy and Power Engineering, Huazhong University of Science and Technology, Wuhan 430074, China.

E-mail address: [tzming@mail.hust.edu.cn](mailto:tzming@mail.hust.edu.cn) (T. Ming).

thermoelectric systems (RTG) used in U.S. space missions and made comparisons between several radioisotope heat sources which were thought much easier to get than the traditional ones. They made a comprehensive analysis of the thermal characteristics and radiation barrier problems. The influence of dimensionless size and external load parameters on a thermoelectric module's efficiency was explored by Yilbas and Sahin [6] who showed that, when the  $ZT_{avg}$  value of the thermoelectric material was constant and the size parameters optimal, the module's maximum efficiency only depended on the temperatures on the hot and cold end. A two-stage solar concentrator designed by Omer and Infield [7] was applied to increase the temperature on a thermoelectric module's hot ends. The device improved the module's stability and efficiency by reducing its sensitivity to light angle as well as keeping the concentration ratio at 20. The two-stage structure not only enhanced the light-gathering efficiency but also confined the air convection intensity in the tube. A device integrating traditional rooftop solar isolation material and a thermoelectric power generator improved by Maneewan et al. [8] was applied to reduce indoor temperature in Thailand. Fans powered by thermoelectric module were used to cool the cold end of the thermoelectric module. The device reduced heat flux into the house and increased the efficiency of the thermoelectric module, which reversely affected the fan's total power and air convection intensity. An idea that incorporated commercially available thermoelectric generators (TEGs) to a water-fed heat exchanger was examined by Zhou et al. [9]. They demonstrated that, when reducing pin length while increasing the number of pins, the resulting reduction in flow resistance was found to facilitate increase in convective heat transfer, as well as in  $\Delta T$ , and thus a great increase in conversion efficiency. A three-dimensional finite element model of a thermoelectric module based on low-temperature thermoelectric material bismuth telluride and medium-temperature thermoelectric material filled-skutterudite was built by Xiao et al. [10]. The numerical simulation results showed that a reasonable thermal design of multi-stage models would take full advantage of the characteristics of thermoelectric materials and effectively improve the performance of power generation.

Generally, the research work related to thermoelectrics could mainly be classified into four categories: (1) The Carnot efficiency was enhanced by increasing the hot side temperature in order to obtain a larger temperature difference between the two ends [7,11]. (2) Researchers made a good effort on finding materials with high  $ZT$  value to improve conversion efficiency of thermoelectric materials. On the other hand, Thomson effect's influence on thermoelectric module efficiency aroused people's attention gradually [12–16]. (3) The structures of thermoelectric devices were optimized to achieve good designs with higher system efficiency. Mathematical analysis and numerical simulation both played important roles in the process [17,18]; and (4), where much research has been done, A lot of research [19–22,23–25] focused on thermoelectric devices applied on certain conditions, such as thermoelectric cooling device in remote desert, thermoelectric power generation device for automobile waste heat utilization, thermoelectric power generation device for space mission and application, which clearly indicates that the research and application of thermoelectric system blossom presently and become much more valuable in the future.

Much investigation has been carried out to examine the thermodynamic performance of thermoelectric devices. But thermal stresses generated in different layers of materials in TEM due to temperature gradients are neglected to a certain extent. Thermal stress induced by high temperature gradient in the device undoubtedly decreases the predicted lifecycle of the module. For solar thermoelectric module, much higher concentration ratio of solar energy will be applied to the hot end of TEM to achieve higher

system efficiency. However, higher temperature of hot end will cause larger thermal stress within the material and among different materials, which will cause serious warp during different layers of materials and thereby significantly decrease the overall efficiency of the TEM. A better understanding of the operating feature of thermoelectric modules with different geometry configurations becomes essential, but seldom can similar work be found in the previous studies. The location of the maximum stress and the level of thermal stress intensity are obscure. Further, thermal stress intensity is the decisive factor for the predicted lifecycle of a thermoelectric device, especially the maximum stress value. To alleviate the hard working condition of the thermoelectric generator devices, a full investigation about the influence of geometry configurations on stress intensity of the module is of great importance. An optimum structure is the one that decreases thermal stress while having little impact or even positive effect on the device's thermoelectric performance. In this paper, a numerical modeling is presented to examine the effect of the conducting strip, ceramic plate and tin soldering geometry configuration on the module's stress level.

## 2. Model description

### 2.1. Physical model

The thermoelectric model tested in the paper is presented in Fig. 1(a), including ceramic plate, conducting strips (copper), thermoelectric pins, and tin soldering. It is considered that the basic parameters of the thicknesses of copper strip, ceramic plates, and tin solder are 0.5, 2.00, and 0.50 mm, respectively. The size of thermoelectric pins is  $3.00 \times 3.00 \times 4.50 \text{ mm}^3$ . The distance between the two pins is 1.00 mm. The parameters of the model, especially the size of the therm-pins, are chosen under the consideration of the common magnitude of commercial thermoelectric products available. The most commonly used  $\text{Bi}_2\text{Te}_3$  is selected for the thermoelectric module and there is no difference in properties as a function of position. Aluminum oxide ceramics ( $\text{Al}_2\text{O}_3$ ) is selected as the material of ceramic plate.

Actually, a single thermoelectric module's lifecycle is random, but the distribution of a large number of thermoelectric modules' lifecycles is ideally normal. In the condition that a large temperature gradient exists, the decisive factor for the lifecycle of a module is thermal stress intensity. As we all know, Young's modulus of aluminum oxide ceramics ( $\text{Al}_2\text{O}_3$ ) and  $\text{Bi}_2\text{Te}_3$  vary greatly, the positions that most possible to crack are those of the interfaces of the copper strips and ceramic plates, and the edges of the thermo-pins. In this paper, we mainly pick up stress intensity data along the three lines shown in Fig. 1, which we respectively mark as Line 1, Line 2 and Line 3, to analyze the overall distribution of thermal stress intensity in the modules. The material properties used in the previous study [3,26] are incorporated in the present simulations, which are listed in Figs. 2–4 and Tables 1 and 2.

### 2.2. Mathematical model

The analysis pertinent to thermoelectric generator is divided into two-sub sections including the thermodynamic analysis and thermal stress formulations.

#### 2.2.1. Thermodynamics and thermoelectricity analysis

##### (1) Governing equations

In this paper a finite element method using thermoelectric element in ANSYS 14.0 is employed to simulate the temperature and

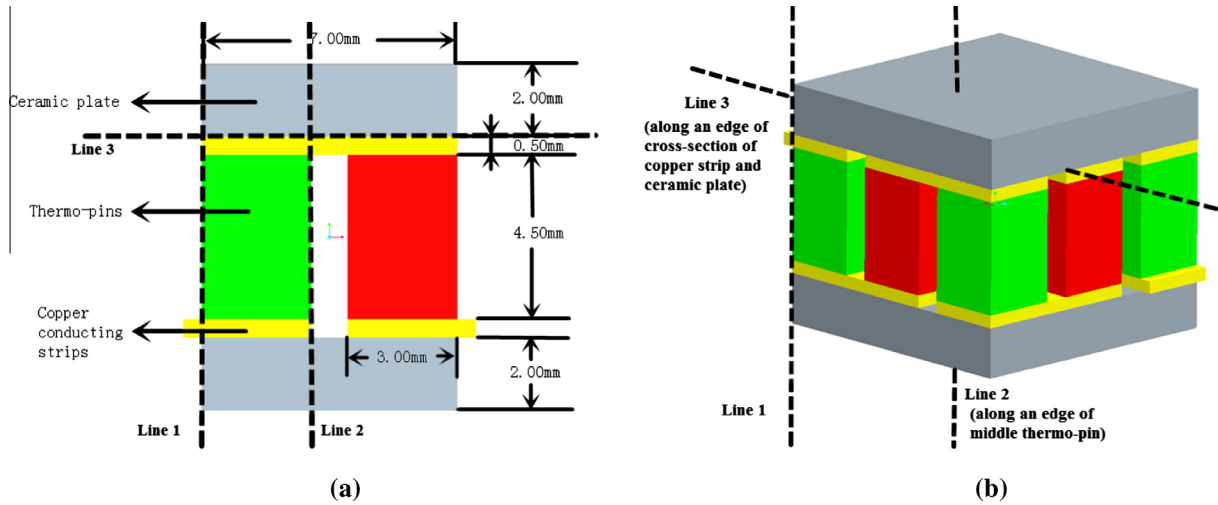


Fig. 1. Geometric dimensions of the thermoelectric model: (a) front view of the referenced thermoelectric power generator and (b) three-dimensional view of thermoelectric module.

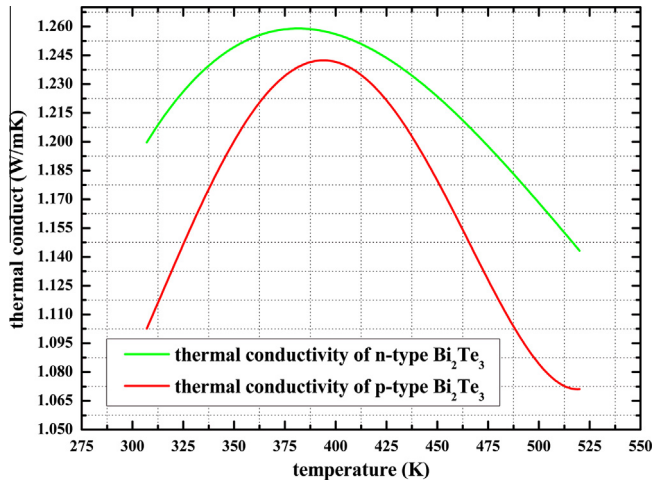


Fig. 2. Thermal conductivity of p-Bi<sub>2</sub>Te<sub>3</sub> and n-Bi<sub>2</sub>Te<sub>3</sub> varying with temperature (307–520 K) [26].

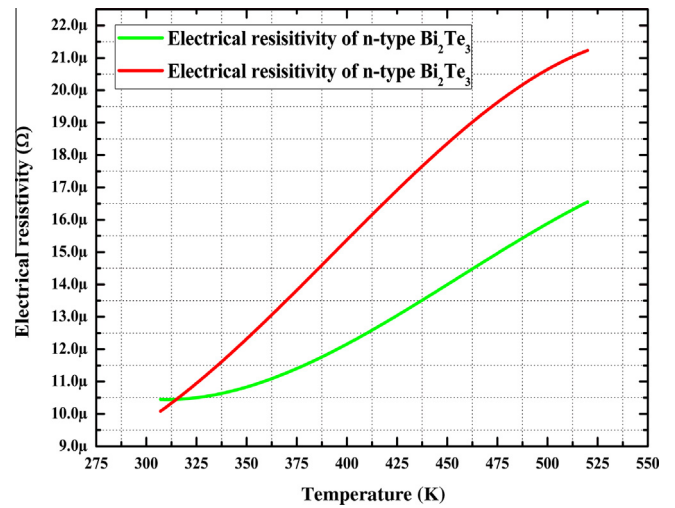


Fig. 4. Electrical resistivity of p-Bi<sub>2</sub>Te<sub>3</sub> and n-Bi<sub>2</sub>Te<sub>3</sub> varying with temperature (307–520 K) [26].

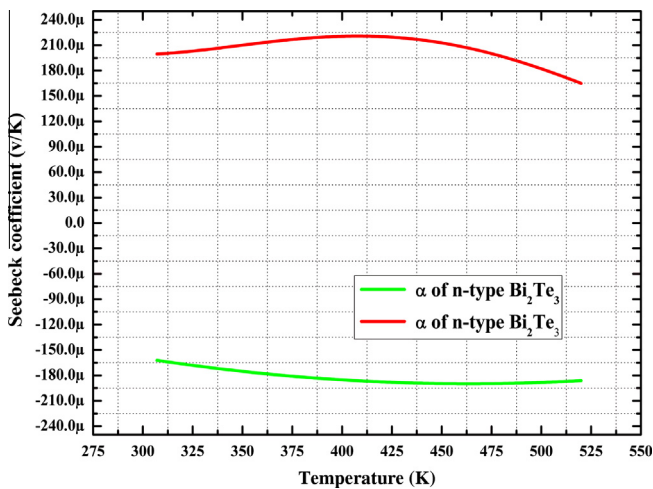


Fig. 3. Seebeck coefficient of p-Bi<sub>2</sub>Te<sub>3</sub> and n-Bi<sub>2</sub>Te<sub>3</sub> varying with temperature (307–520 K) [26].

Table 1  
Properties of Bi<sub>2</sub>Te<sub>3</sub> [3].

Temperature (K)	Thermal expansion (/K)	
297	8.0e–6	
304.3	1.01e–5	
365	1.21e–5	
451	1.24e–5	
613	1.32e–5	
793	1.33e–5	
864	1.41e–5	
Temperature (K)	Poisson's ratio	Young's modulus (pa)
200	0.23	6.5e10
300	0.23	6.3e10
400	0.23	6.2e10
500	0.23	6.0e10
600	0.23	5.9e10

**Table 2**  
Properties of other materials [3].

Material	Thermal expansion (/K)	Poisson's ratio Young's	Young's modulus (pa)
Cu	17.7e-6	0.326	11.9e10
Al <sub>2</sub> O <sub>3</sub>	8.8e-6	0.3	35e10
Sn	2.0e-6	0.33	5.44e10
Material	Thermal conductivity (W/(m K))	Electrical resistivity (Ω m)	
Cu	300	2.5e-8	
Sn	80	1.14e-7	

electric field in thermoelectric modules. Equations that couple temperature  $T$  and electric potential  $V$  are:

$$\nabla(k\nabla T) + \rho \mathbf{J}^2 - T\mathbf{J} \cdot \left[ \left( \frac{\partial \alpha}{\partial T} \right) \nabla T + (\nabla \alpha)_T \right] = 0 \quad (1)$$

$$\nabla \cdot \mathbf{J} = 0 \quad (2)$$

where

$$\mathbf{J} = -\sigma \left[ \nabla \left( \frac{\mu}{e} + V \right) + \alpha \nabla T \right] \quad (3)$$

$$\mathbf{q} = \alpha T \mathbf{J} - k \nabla T \quad (4)$$

In the equations above,  $k$  is thermal conductivity at zero current; vector  $\mathbf{J}$  is the electric current per unit area;  $\rho$  is electric resistivity;  $\sigma = 1/\rho$  is electric conductivity;  $\alpha$  is Seebeck coefficient;  $\mu$  is the chemical potential; and  $e$  is the charge of charged particle. Note that  $k$ ,  $\rho$ ,  $\alpha$ , and  $\sigma$  are functions of temperature.

Thermoelectric modules are not ideally one dimensional structures. Eq. (1) reflects the multidimensional effects that can be obvious in interfaces of the modules. Eqs. (1) and (2) form a system coupled with two partial differential equations with two dependent variables, the temperature and electric potential. Eq. (1) can be separated into four parts, which respectively reflect the magnitude of thermal energy transferred by conducting, Joule heat, heat absorbed by Peltier effect, and heat absorbed or released by Thomson effect.

## (2) Boundary conditions

Some reasonable assumptions are made to simplify mathematical model without too much deviation from the real conditions.

- All the surfaces except the hot end and cold end are considered to be heat insulation.
- Heat convection and heat radiation on all the surfaces are neglected.
- No differences in properties as a function of position exist.
- Electrical contact resistance and thermal contact resistance are not taken into consideration. According to Ref. [26], when pins lengths are larger than 4.0 mm, their impact on the performance of the thermoelectric module is very small.

Note that all the assumptions introduced above are aimed at excluding other unimportant factors that have little effect on the results and at avoiding analyzing two or more factors simultaneously.

The boundary conditions for thermoelectric thermodynamics analysis are shown as follows.

The actual generator is cooled by a heat sink connected to the cold end, with water serving as the working medium. Here, the cooling of the generator is assumed to be perfect and the first boundary condition is applied to the cold end of the thermoelectric module with a fixed value of 300 K (about 27 °C). The assumption is reasonable, for TEG model can be seen as a temperature buffer

that slight temperature changes in the cold end can be neglected. Then, a specified temperature is applied to the cold end:

$$T_C = 300 \text{ K} \quad (5)$$

In this paper, the total heat flows were constant, aiming at excluding the influence of the unrelated factors. In addition, the value of heat fluxes for all parts were chosen as  $q_{\text{avg}} = 33,058 \text{ W/m}^2$  except Sections 3.2 and 3.4. In Section 3.2, to make the comparison valid, the total heat flows in the hot end were assumed to be constant, 0.21 W ( $q_{\text{avg}} = 10,000 \text{ W/m}^2$  for  $D_{\text{Leg-sp}} = 1.0 \text{ mm}$ ) for all cases, but the heat fluxes varied from case to case. In Section 3.4, a heat flux  $q_{\text{avg}} = 10,000 \text{ W/m}^2$  was applied to ensure that the temperature in the module was lower than the fusing point of tin. The magnitude of heat fluxes chosen in the paper was common in the electronic components. The corresponding peak temperature on the hot end of TE legs was no more than 550 K. Specified heat flow was applied to the hot end:

$$q_{\text{avg}} = 33058 \text{ W/m}^2 \text{ (for Sections 3.1 and 3.3)}$$

$$\text{or } q_{\text{avg}} = 10000 \text{ W/m}^2 \text{ (for Sections 3.2 and 3.4)} \quad (6)$$

Where both temperature and heat flux can be functions of position on the surface; in fact, the influence of inhomogeneous heat flux on the devices' overall performance is partially presented and will be fully explored in future study. For now, here, the total heat flow is constant, aiming at excluding the influence of the unrelated factors. In addition, the value of heat flux on the hot end will vary with different cases.

Reference voltage was applied to a point on the copper strip surface

$$E(x = 0, y = 0, z = 0) = 0 \quad (7)$$

Because all the surfaces of the legs are exposed to electric insulating gas, the current must be parallel to the surfaces.

$$\mathbf{J} \cdot \mathbf{n} = 0 \quad (8)$$

After discretizing the calculating domain and replacing the PDEs by algebraic equations, we manage to get the temperature and electric fields in the module.

## 2.2.2. Thermal stress analysis

### (1) Governing equations

Because thermal conductivity of material is a function of temperature, a thermoelectric module is not strictly one-dimensional. Thermodynamic and mechanical characteristics in the  $z$  axis direction are nonlinear. We neglect the part of heat converted to electric energy, because this part is only a small portion of the total heat flux and it would not virtually affect the conclusions. The thermodynamic equation is presented as

$$\frac{\partial}{\partial x} \left[ k \frac{\partial T}{\partial x} \right] + \frac{\partial}{\partial y} \left[ k \frac{\partial T}{\partial y} \right] + \frac{\partial}{\partial z} \left[ k \frac{\partial T}{\partial z} \right] = 0 \quad (9)$$

where  $\kappa = f(T)$  and  $T = f(x, y, z)$ . A temperature field is obtained by numerical simulation which is applied to thermal stress analysis.

A similar thermal stress analysis method utilized in Refs. [1,3] is employed to evaluate the thermal intensity in the model. In this paper, the analysis of the thermoelectric generator is divided into two-sub parts including the thermodynamic analysis and thermal stress formulations. Temperature field acquired in the thermodynamic analysis is used to calculate the thermal stress field in the model. There is no doubt that temperature field and deformation will influence each other. But it should be mentioned that, the temperature field will significantly affect the thermal stress field while

the counteractive is not obvious, for the deformation is quite small when compared with the model geometry magnitude.

To identify the displacement–strain relations, dimensionless equations are listed:

$$\bar{\epsilon}_{xx} = \frac{\partial \bar{u}}{\partial \bar{x}}, \quad \bar{\epsilon}_{yy} = \frac{\partial \bar{v}}{\partial \bar{y}}, \quad \bar{\epsilon}_{zz} = \frac{\partial \bar{w}}{\partial \bar{z}} \quad (10)$$

$$\bar{\epsilon}_{xy} = 0.5 \left( \frac{\partial \bar{u}}{\partial \bar{y}} + \frac{\partial \bar{v}}{\partial \bar{x}} \right), \quad \bar{\epsilon}_{yz} = 0.5 \left( \frac{\partial \bar{w}}{\partial \bar{y}} + \frac{\partial \bar{v}}{\partial \bar{z}} \right), \quad \bar{\epsilon}_{zx} = 0.5 \left( \frac{\partial \bar{w}}{\partial \bar{x}} + \frac{\partial \bar{u}}{\partial \bar{z}} \right) \quad (11)$$

A nonsymmetrical Jacobian matrix expresses stress–strain relation in a dimensionless form:

$$\begin{Bmatrix} \bar{\sigma}_{xx} \\ \bar{\sigma}_{yy} \\ \bar{\sigma}_{zz} \\ \bar{\sigma}_{yz} \\ \bar{\sigma}_{zx} \\ \bar{\sigma}_{xy} \end{Bmatrix} = \frac{\bar{E}}{(1+\nu)(1-2\nu)} \times \begin{bmatrix} 1-\nu & \nu & \nu & 0 & 0 & 0 \\ \nu & 1-\nu & \nu & 0 & 0 & 0 \\ \nu & \nu & 1-\nu & 0 & 0 & 0 \\ 0 & 0 & 0 & 1-2\nu & 0 & 0 \\ 0 & 0 & 0 & 0 & 1-2\nu & 0 \\ 0 & 0 & 0 & 0 & 0 & 1-2\nu \end{bmatrix} \begin{Bmatrix} \bar{\epsilon}_{xx} \\ \bar{\epsilon}_{yy} \\ \bar{\epsilon}_{zz} \\ \bar{\epsilon}_{yz} \\ \bar{\epsilon}_{zx} \\ \bar{\epsilon}_{xy} \end{Bmatrix} - \begin{Bmatrix} 1 \\ 1 \\ 1 \\ 0 \\ 0 \\ 0 \end{Bmatrix} \frac{\bar{\alpha} E T}{1-2\nu} \quad (12)$$

The mechanical and thermodynamic equations are coupled to obtain the temperature and thermal stress fields in the module (see Tables 3–6).

The First Strength Theory (the Maximum Normal Stress Theory), having good adaptability to access ultimate strength of brittle materials under three-dimensional stress state, is adopted to evaluate the stress intensity. If all the three principal stress values do not equal zero, we mark them  $\sigma_1$ ,  $\sigma_2$ , and  $\sigma_3$  (supposing  $\sigma_1 \geq \sigma_2 \geq \sigma_3$ ). Then we get maximum normal stress  $\sigma_{\max}$ , the minimum normal stress  $\sigma_{\min}$ , and maximum shear stress  $\tau_{\max}$ :

$$\sigma_{\max} = \sigma_1, \quad \sigma_{\min} = \sigma_3, \quad \tau_{\max} = \frac{|\sigma_1 - \sigma_3|}{2} \quad (13)$$

(2) Boundary conditions

Boundary conditions for thermodynamic analysis are listed in Eqs. (7) and (8). The corresponding heat flux magnitude is common in electronic products. Very high heat flux leads to a considerable thermal stress level in the module. In this section, a unicouple

model is employed to examine the stress field. To verify the reliability of final results, separate series of calculations ( $q_{\text{avg}} = 10,000 \text{ W/m}^2$ ,  $q_{\text{avg}} = 20,000 \text{ W/m}^2$ ) are executed while other conditions remain the same.

The boundary conditions for thermal stress analysis are shown below in Eqs. (9)–(12). On surfaces  $z = 7.5 \text{ mm}$  (hot end) and  $z = 0.0 \text{ mm}$  (cold end), strains in  $z$  direction and all shear deformations are set to zero:

$$\bar{\epsilon}_{zz}(z = 7.5 \text{ mm}) = \bar{\epsilon}_{xz}(z = 7.5 \text{ mm}) = \bar{\epsilon}_{yz}(z = 7.5 \text{ mm}) = 0 \quad (14)$$

$$\bar{\epsilon}_{zz}(z = 0.0 \text{ mm}) = \bar{\epsilon}_{xz}(z = 0.0 \text{ mm}) = \bar{\epsilon}_{yz}(z = 0.0 \text{ mm}) = 0 \quad (15)$$

On surfaces  $x = 3.0 \text{ mm}$  (front face) and  $x = 0.0 \text{ mm}$  (back face), strains in  $x$  direction and all shear deformation are set to zero:

$$\bar{\epsilon}_{xx}(x = 3.0 \text{ mm}) = \bar{\epsilon}_{xy}(x = 3.0 \text{ mm}) = \bar{\epsilon}_{xz}(x = 3.0 \text{ mm}) = 0 \quad (16)$$

$$\bar{\epsilon}_{xx}(x = 0.0 \text{ mm}) = \bar{\epsilon}_{xy}(x = 0.0 \text{ mm}) = \bar{\epsilon}_{xz}(x = 0.0 \text{ mm}) = 0 \quad (17)$$

Here we restrain the front and back faces to show they are symmetrical planes. The results can be used to estimate stress field in a whole module, especially for couples in the center of the model.

All the boundary conditions are set to be similar to the real ones.

2.3. Computation method

In order to test the grid-independence performance of the grid system in numerical simulation, three test cases of the same boundary conditions ( $q_{\text{avg}} = 33,058 \text{ W/m}^2$ ) with grid number being 27,956, 60,352, and 83,599 were examined (for single couple thermo-pins, the respective numbers were 7200, 9216, and 17,070). When the external resistance was chosen as  $0.055 \Omega$ , numerical simulation results indicated that the external voltages respectively were 0.0735, 0.0734, and 0.0733 V. Another series of tests were carried out to check the stress intensity in single couple thermo-pins, the respective grid numbers were 7200, 9216, and 17,070. Stress intensities of two intersection points on Line 3 are checked. For the first point, the stress intensities were 2.17e9, 2.18e9, and 2.18e9 pa, respectively. For the second point, the stress intensities were 2.22e9, 2.22e, and 2.22e9 pa. We found that the deviation was negligible, which demonstrated that numerical calculations were grid-independent for these cases. Here, a grid number of 60,352 shown in Fig. 5 was thus selected as the mesh system in this paper.

A grid system the same as the one employed in thermodynamics and thermoelectric analysis was applied to thermal stress analysis. Finite element method (FEM) calculations were performed by using general thermoelectric analysis package ANSYS 14.0. Thermal solid brick 8node 70 element and structural solid brick 8node 185 element were used to discretize the computational domain. The iterations continued until the relative errors of heat flow and electric current are both below  $1 \times 10^4$ . In this section we chose the model with a coupled thermo-pin as the reference for these considerations: (1) saved computing resource; and (2) when we restrained expansion displacement in hot and cold ends surface, there was little difference in results between one coupled thermo-pin and many coupled ones.

3. Results and discussion

Temperature and thermal stress distributions developed in the thermoelectric power generator module were investigated and the influences of ceramic plates, copper conducting strips, tin soldering geometry configurations, and the distance between thermo-pins on the thermal stress levels were examined. In Fig. 6(a1) and

**Table 3**  
Peak  $\sigma_1$  on the lines for different ceramic plate thicknesses.

Ceramic plate thickness (mm)	Peak $\sigma_1$ on Line 1 (pa)	Peak $\sigma_1$ on Line 3 (pa)
0.50	1.25e9	1.26e9
1.00	1.32e9	1.31e9
1.50	1.37e9	1.32e9
2.00	2.10e9	2.29e9
2.50	1.20e9	1.34e9

**Table 4**  
Peak  $\sigma_1$  on the lines for different thermo-pins distances.

Thermo-pins distance (mm)	Peak $\sigma_1$ on Line 1 (pa)	Peak $\sigma_1$ on Line 2 (pa)	Peak $\sigma_1$ on Line 3 (pa)
0.50	1.47e8	1.15e8	1.27e8
1.00	1.57e8	1.23e8	1.36e8
1.50	1.68e8	1.31e8	1.47e8
2.00	1.78e8	1.40e8	1.55e8

**Table 5**  
Peak  $\sigma_1$  on the lines for different copper conducting strip thicknesses.

Copper conducting strip thickness (mm)	Peak $\sigma_1$ on Line 1 (pa)	Peak $\sigma_1$ on Line 3 (pa)
0.25	1.18e9	1.37e9
0.50	2.10e9	2.29e9
0.75	1.23e9	1.31e9
1.00	1.25e9	1.29e9

**Table 6**  
Peak  $\sigma_1$  on the lines for different tin soldering thicknesses.

Tin soldering thickness (mm)	Peak $\sigma_1$ on Line 1 (pa)	Peak $\sigma_1$ on Line 2 (pa)	Peak $\sigma_1$ on Line 3 (pa)
0.0	1.57e8	1.46e8	1.341e8
0.5	1.55e8	1.44e8	1.330e8
1.0	1.48e8	1.39e8	1.285e8
1.5	1.39e8	1.30e8	1.206e8
2.0	1.28e8	1.20e8	1.105e8
2.5	1.15e8	1.09e8	0.994e8

(b1), there was a referenced module with basic geometrical dimensions:  $D_{\text{Cer}} = 2.00$  mm,  $\text{Leg\_Sp} = 0.50$  mm,  $t_{\text{Cu}} = 0.50$  mm,  $t_{\text{Solder}} = 0.00$  mm, and  $q_{\text{avg}} = 10,000$  W/m<sup>2</sup>. The other modules from (a2) and (b2) to (a5) and (b5) were all only one dimensional variations.

It is obvious in Fig. 6(a) that temperature distributions are nearly 1-D except for the cases where the modules have a soldering layer and the highest temperature in the modules fluctuates insignificantly. As demonstrated in Fig. 6(b), thermal stress distributions in thermoelectric module vary remarkably. Compared with the referenced module, the added tin soldering layer in Fig. 6(b2) alleviates the peak thermal stress intensity and shifts the high thermal stress region from the side to the center of the modules. As shown in Fig. 6(b3), a thinner ceramic layer leads to a higher stress intensity in the ceramic layer but has little influence on other parts of the module. Fig. 6(b4) indicates that greater leg space distance deteriorates the work condition of the module by adding the peak thermal stress. But it still does a little good on the module by dispersing the high thermal stress regions. An analysis on the influential factors on the performance of the module, and the ways to improve its performance are presented below.

### 3.1. The influence of ceramic plate thickness

Fig. 7 shows the temperature and normal stress distributions on Line 1 for various ceramic plate thicknesses. Because  $\sigma_1$  is much larger than  $\sigma_2$  and  $\sigma_3$ , we can utilize  $\sigma_1$  to predict the maximum thermal stress intensity level in the module. Inasmuch as maximum temperature surpasses the temperature range of material thermodynamics properties available, the temperature gradient near the hot end of the thermo-pins is constant. But this phenomenon has little impact on the discussion. It can be observed that the maximum thermal stress emerges on the top surface and changes relatively slightly in this ceramic plate. In the interface of ceramic

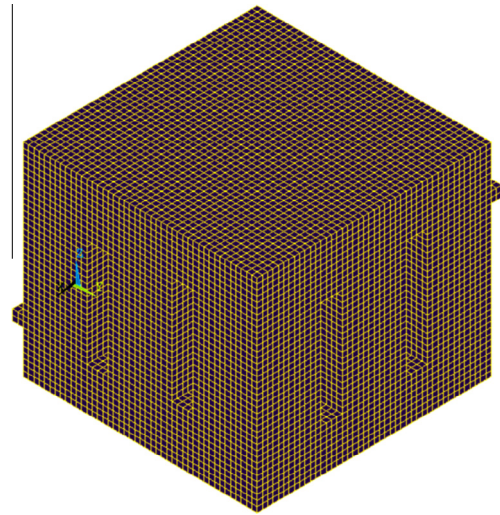


**Fig. 5.** Grid system of the thermoelectric module.

plate and copper conducting strip, the most likely place for a crack, the corresponding normal stresses are 1.25e9, 1.32e9, 1.37e9, 2.10e9, and 1.20e9 pa with ceramic plate thicknesses being 0.50, 1.00, 1.50, 2.00, and 2.50 mm, respectively. It can be concluded that  $\sigma_{\text{max}}$  increases with increasing ceramic plate thickness and then reverses at somewhere around 2.00 mm. To alleviate thermal stress in the module, a smaller or larger ceramic plate thickness should be chosen.

Temperature and normal stress distributions along Line 3 for various ceramic plate thicknesses are presented in Fig. 8. The maximum thermal stress appears on position  $y = 2.50$  mm or  $y = 4.50$  mm, which agrees well with the temperature gradient distribution. With ceramic plate thicknesses varying at 0.50, 1.00, 1.50, 2.00, and 2.50 mm, the respective normal stresses are 1.26e9, 1.31e9, 1.32e9, 2.29e9, and 1.34e9 pa. Line 3 is in the interface, one relatively weak and soft, of the ceramic plate and copper conducting strip. Similar results are found on Line 1 and Line 3. Adding ceramic plate is helpful to reduce the possibility of cracking.

Smaller and larger ceramic plate thicknesses both would be of benefit to the lifecycle of thermoelectric module. To enforce the protective effect of a ceramic plate, a larger ceramic plate thickness ( $\geq 2.5$  mm) is chosen to ensure the reliability of the device.

### 3.2. The influence of the thermo-pins distance

The distance between thermo-pins is another important factor that affecting thermal stress distribution. In this sector we examine the influence of various thermo-pins distances on the module's thermal stress level. To exclude the influence of the unrelated factors, the total heat flow in the hot end is assumed to be 0.21 W ( $q_{\text{avg}} = 10,000$  W/m<sup>2</sup> for  $D_{\text{Leg\_sp}} = 1.0$  mm) for all cases, smaller than 0.69 W ( $q_{\text{avg}} = 33,058$  W/m<sup>2</sup>) for the section above.

Fig. 9 shows the maximum thermal stress on Line 1 which emerges on the surface of thermoelectric module regardless of thermo-pins distance. With the thermo-pins in-between distance varying from 0.50 to 2.00 mm at steps of 0.50 mm, the maximum thermal stresses are 1.47e8, 1.57e8, 1.68e8, and 1.78e8 pa, respectively. It is obvious that increasing the thermo-pins' distance from each other adds the possibility of cracking. For weaker strength on the interface of ceramic plate and copper conducting strip, special attention should be paid to the stress intensity there. The maximum thermal stresses on the interface are 1.15e8, 1.23e8, 1.31e8, and 1.40e8 pa, respectively. It can be observed that

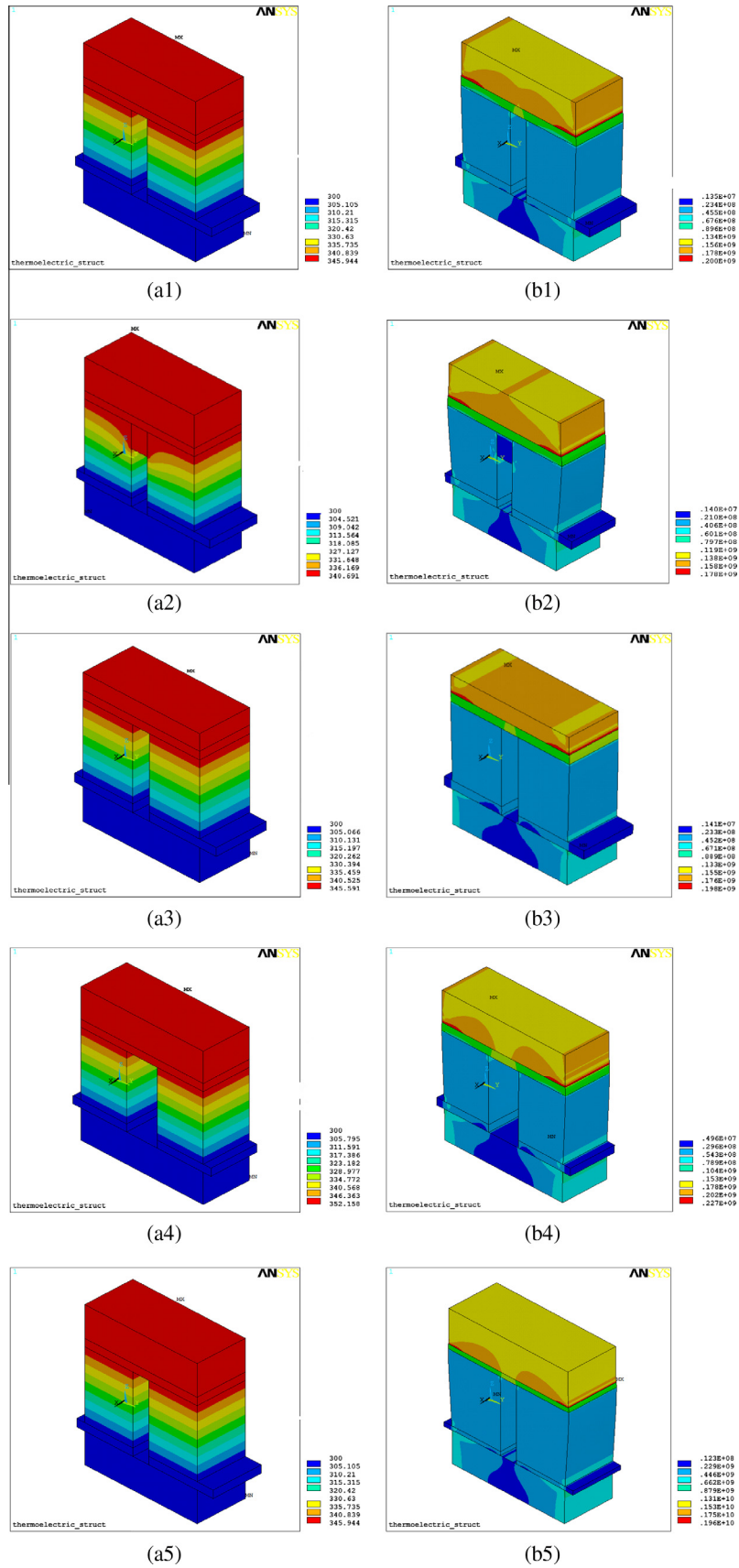


**Fig. 6.** Typical simulation results of the thermoelectric models for various geometries: (a) temperature distribution and (b) stress intensity distribution. (a1) and (b1) are referenced module; (a2) and (b2)  $t_{\text{solder}} = 1.50 \text{ mm}$ ; (a3) and (b3)  $D_{\text{Cer}} = 0.10 \text{ mm}$ ; (a4) and (b4)  $\text{Leg\_Sp} = 1.50 \text{ mm}$ ; (a5) and (b5)  $t_{\text{Cu}} = 0.25 \text{ mm}$ .

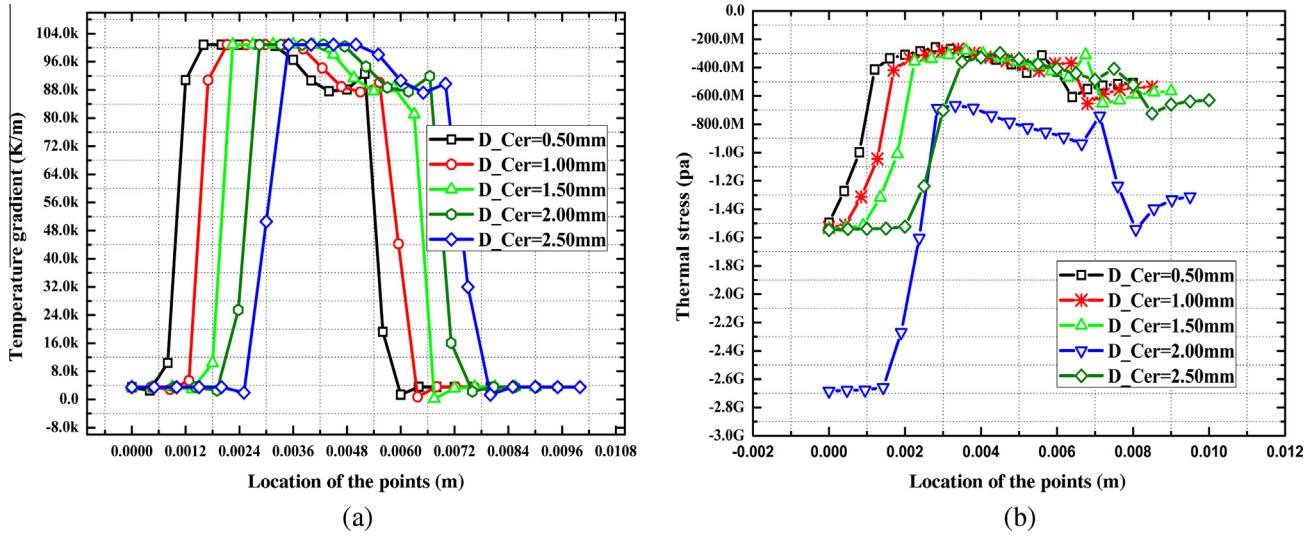


Fig. 7. The influence of ceramic plate thickness on the thermoelectric module (Line 1): (a) distribution of temperature gradient and (b) distribution of  $\sigma_1$ .

increasing the thermo-pins' distance raises maximum thermal stress on Line 1. The phenomenon can be reasoned as two factors. On one hand, larger leg-distance results in higher overall thermal resistance per surface area and a higher temperature gradient. On the other hand, rapid change in local structure leads to stress concentration.

Compared with Fig. 9, the thermal stress distribution of Line 2 as shown in Fig. 10 is similar in variation trend with that of Line 1 but is relatively higher. This is due to the stress concentration caused by a more complicated local structure around Line 2. Thereby, increasing the distance between the thermo-pins will increase the thermal stress within the thermoelectric module.

Fig. 11 demonstrates temperature gradient and thermal stress distributions on Line 3 for various thermo-pins distances. The maximum thermal stress appears on the side faces of the thermo-pins' near their midsections. With the thermo-pins distances being 0.50, 1.00, 1.50, and 2.00 mm, the maximum thermal stresses are 1.27e8, 1.36e8, 1.47e8, and 1.55e8 pa, respectively. A larger thermo-pins' distance causes a higher stress level. It can be concluded that a smaller thermo-pins distance should be chosen to

alleviate thermal stress and prolong the lifecycle of thermoelectric module.

### 3.3. The influence of copper conducting strip thickness

Copper is a kind of plastic material. Adding the copper thickness will increase allowable maximum strain. On the other hand, it will aggravate stress intensity between materials with different expansion coefficient. Thereby, a reasonable copper strip thickness is suggested to be applied.

Fig. 12 shows temperature gradient and thermal stress distributions on Line 1 for various copper strip thicknesses. When the copper strip thickness are 0.25, 0.50, 0.75, and 1.00 mm, the  $\sigma_1$  on the interface of ceramic plate and copper strip are 1.18e9, 2.10e9, 1.23e9, and 1.25e9 pa, respectively. The maximum thermal stress occurs on the surface of the ceramic plate for its much larger Young's modulus. In the case when the copper thickness is 0.50 mm, the module has its maximum thermal stress. When copper thickness is larger or smaller than 0.50 mm, there is little difference between the results.

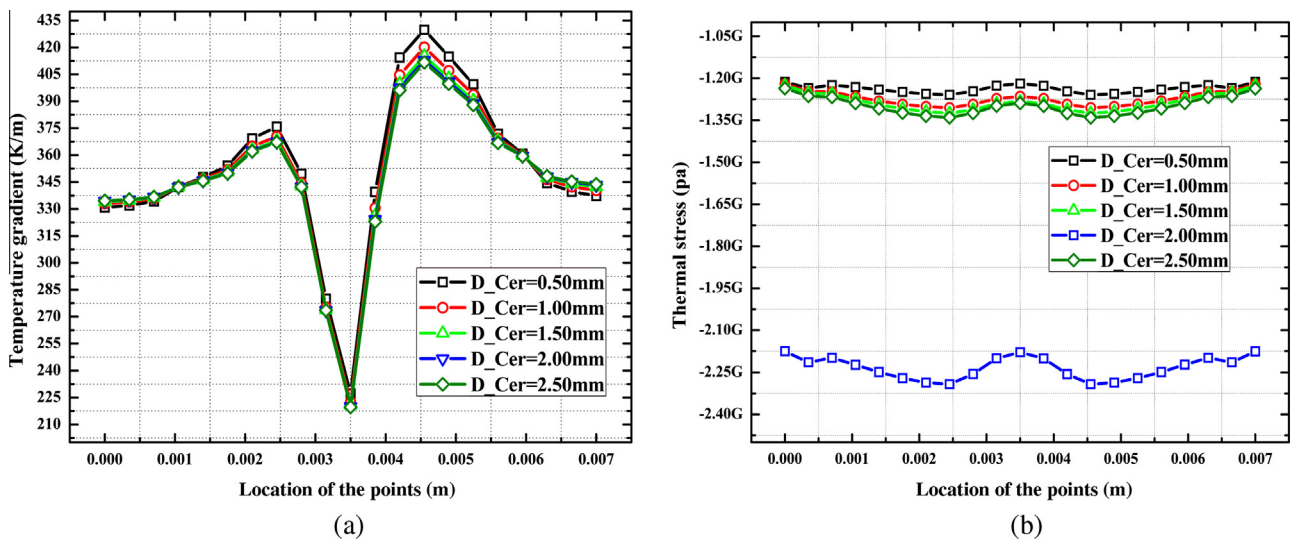


Fig. 8. The influence of ceramic plate thickness on the thermoelectric module (Line 3): (a) distribution of temperature gradient and (b) distribution of  $\sigma_1$ .



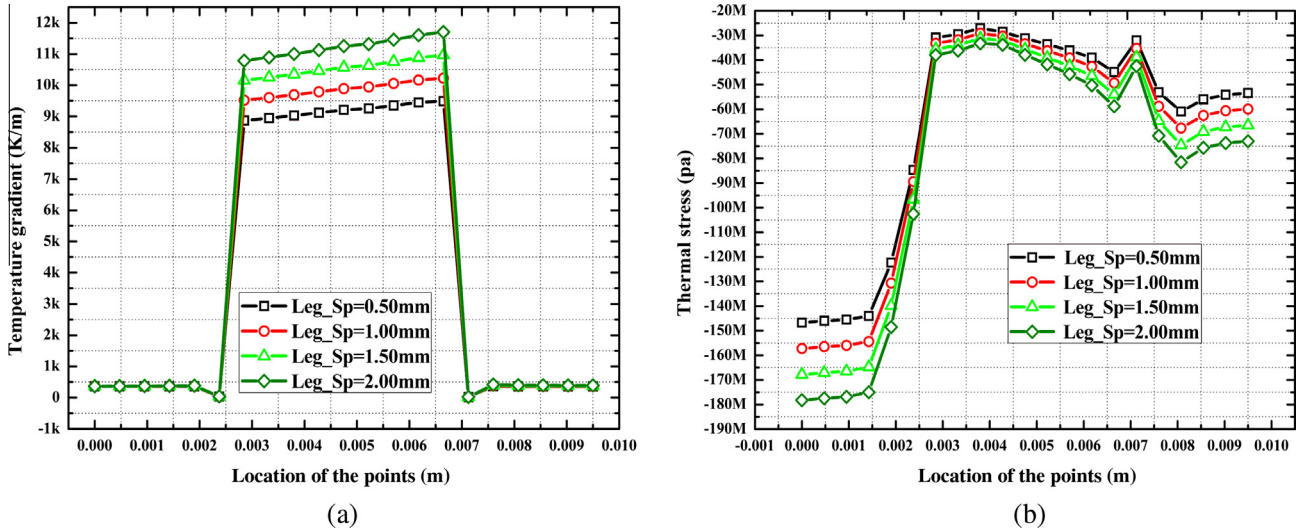


Fig. 9. The influence of thermo-pins distance on the thermoelectric module (Line 1): (a) distribution of temperature gradient and (b) distribution of  $\sigma_1$ .

Fig. 13 shows the thermal stress distribution along Line 2 for various copper thicknesses, which is similar to the situation on Line 1 but a bit larger for stress concentration induced by a more complicated strain condition.

Fig. 14 shows temperature gradient and thermal stress distributions on Line 3 for various copper strip thicknesses. Note that the variations of temperature gradient and thermal stress distributions on Line 3 become increasingly more stable with increasing copper thickness. A larger copper thickness is good for equilibrium temperature distribution. For conditions that copper thicknesses are 0.25, 0.50, 0.75, and 1.00 mm, the maximum thermal stresses are 1.37e9, 2.29e9, 1.31e9, and 1.29e9 pa, respectively. Except for the case of copper thickness being 0.50 mm, there is little difference between other conditions, which is similar to the situation on Line 1 and Line 2.

A larger ( $\geq 0.50$  mm) or a smaller ( $\leq 0.50$  mm) copper thickness can reduce stress level in the module. In practice, a smaller thickness is a better choice to save copper material.

### 3.4. The influence of tin soldering thickness

In this section, a tin soldering layer, in addition to the TE model, was used to fill the gap between the two TE legs. A series of simulations were carried out to test the influence of the Sn soldering thickness on the performance of the TEG model, both in thermodynamics and thermal stress analysis. A heat flux  $q_{avg} = 10,000 \text{ W/m}^2$  is applied to insure that the temperature in the module is lower than the fusing point of tin. Besides, tin soldering thickness' impact on the efficiency of thermoelectric module is investigated.

Fig. 15 shows the temperature gradient and thermal stress distributions on Line 1 for various tin soldering thicknesses. The maximum thermal stress appears on top surface of the ceramic plate. With the tin soldering thicknesses being 0.00, 0.50, 1.00, 1.50, 2.00, and 2.50 mm, the respective maximum thermal stresses are 1.57e8, 1.55e8, 1.48e8, 1.39e8, 1.28e8, and 1.15e8 pa. On the interface of the ceramic plate and the copper conducting strip, the most possible position for cracking, the thermal stresses are 1.23e8, 1.21e8, 1.14e8, 1.00e8, and 9.00e7 pa, respectively. Tin soldering material is effective in alleviating thermal stress in a thermoelectric module.

Fig. 16 shows the temperature gradient and thermal stress distributions on Line 2 for various tin soldering thicknesses. With the tin soldering thicknesses being 0, 0.50, 1.00, 1.50, 2.00, and

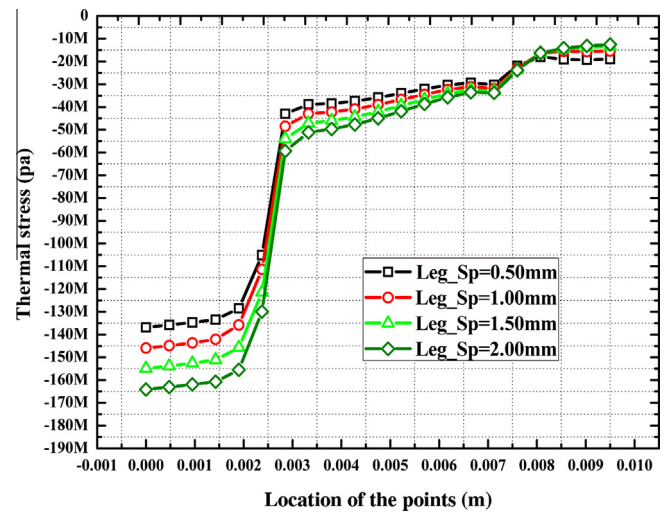
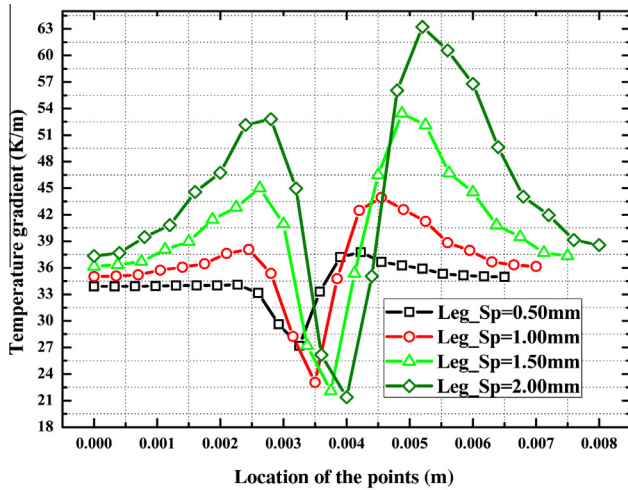


Fig. 10. Distribution of  $\sigma_1$  for various thermo-pins distance on Line 2.

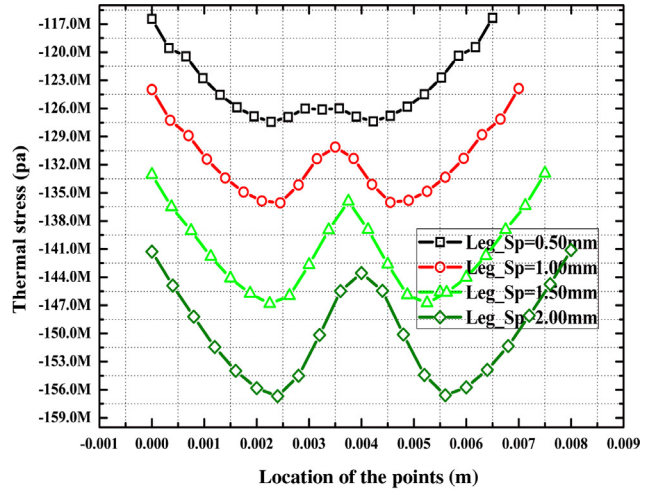
2.50 mm, the respective maximum thermal stresses are 1.46e8, 1.44e8, 1.39e8, 1.30e8, 1.20e8, and 1.08e8 pa. On the interface of the ceramic plate and the copper conducting strip, the thermal stresses are 1.30e8 pa, 1.28e8, 1.23e8, 1.15e8, and 9.50e7 pa, respectively. Compared with the module without tin soldering, the thermal stress distribution difference between Line 1 and Line 2 is much bigger, for tin soldering changes the temperature distribution in the module greatly.

Fig. 17 shows temperature gradient and thermal stress distributions along Line 3 for various tin soldering thicknesses. For different tin soldering thicknesses, the maximum thermal stresses on Line 3 are 1.341e8, 1.330e8, 1.285e8, 1.206e8, 1.105e8, and 9.937e7 pa, respectively. Line 3 is located in the interface of the ceramic plate and the copper conducting strip, the weakest position for cracking, which should be paid special attention to.

Taking an overall consideration of the thermal stress distribution along Line 1, Line 2 and Line 3, thicker tin soldering actually makes for a prolonged lifecycle of a thermoelectric generator module.

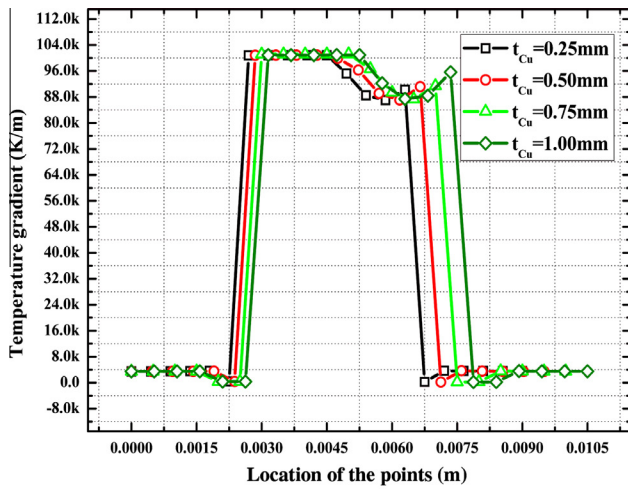


(a)

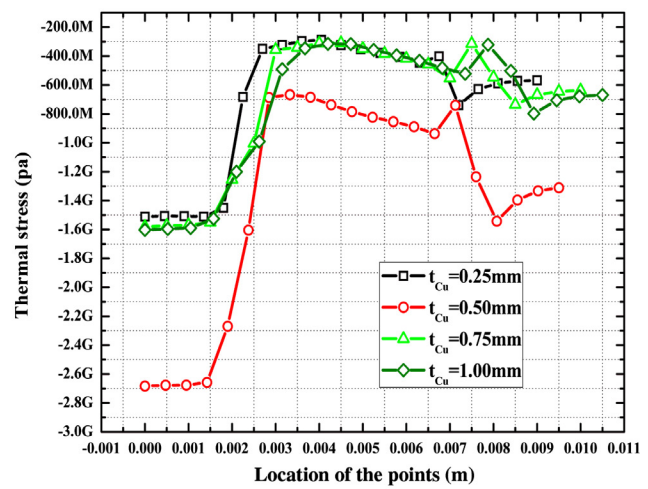


(b)

Fig. 11. The influence of thermo-pins distance on the thermoelectric module (Line 3): (a) distribution of temperature gradient and (b) distribution of  $\sigma_1$ .



(a)



(b)

Fig. 12. The influence of copper conducting strip thickness on the thermoelectric module (Line 1): (a) distribution of temperature gradient and (b) distribution of  $\sigma_1$ .

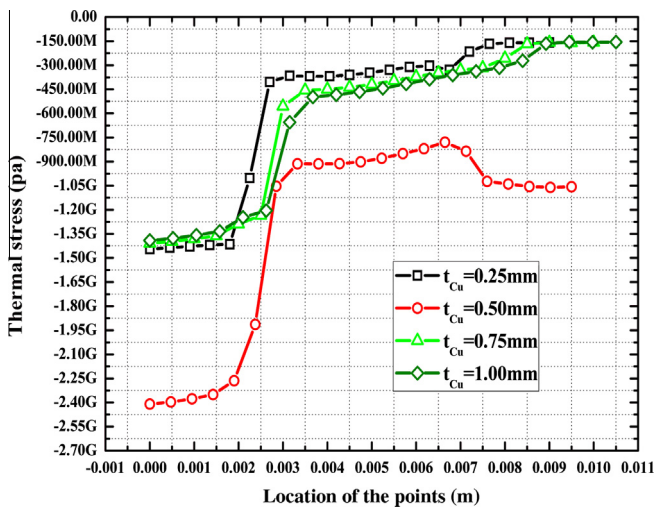


Fig. 13. Distribution of  $\sigma_1$  with various copper conducting strip thickness on Line 2.

Another numerical simulation has been performed to check the influence of tin soldering thickness on maximum power output and maximum electric voltage of the thermoelectric module. The result is shown in Fig. 18.

Though the voltage output decreases (Fig. 18), increasing the tin soldering thickness will increase the power output of the thermoelectric module within limits, for the thermal conductivity of tin is much larger than  $\text{Bi}_2\text{Te}_3$ . It can be reasoned as follows. Tin soldering greatly changes the temperature distribution in the module and increases the temperature gradient in the thermo-pins. Though the tin soldering layer reduces the total thermal resistance of the device, the TE electrical resistance also decreases. There must be an optimum tin soldering thickness where the power output of the thermoelectric module reaches its peak value.

Choosing a suitable tin soldering thickness (like 0.50 mm) will not only alleviate the thermal stress intensity in the module, but also increase the thermal efficiency.

The issue of thermal stress concentration phenomenon occurs in many cases when the heat flux on the receiver is very high or the temperature gradient is very high in the material or across the interface of materials. To consider this issue, to some extent,

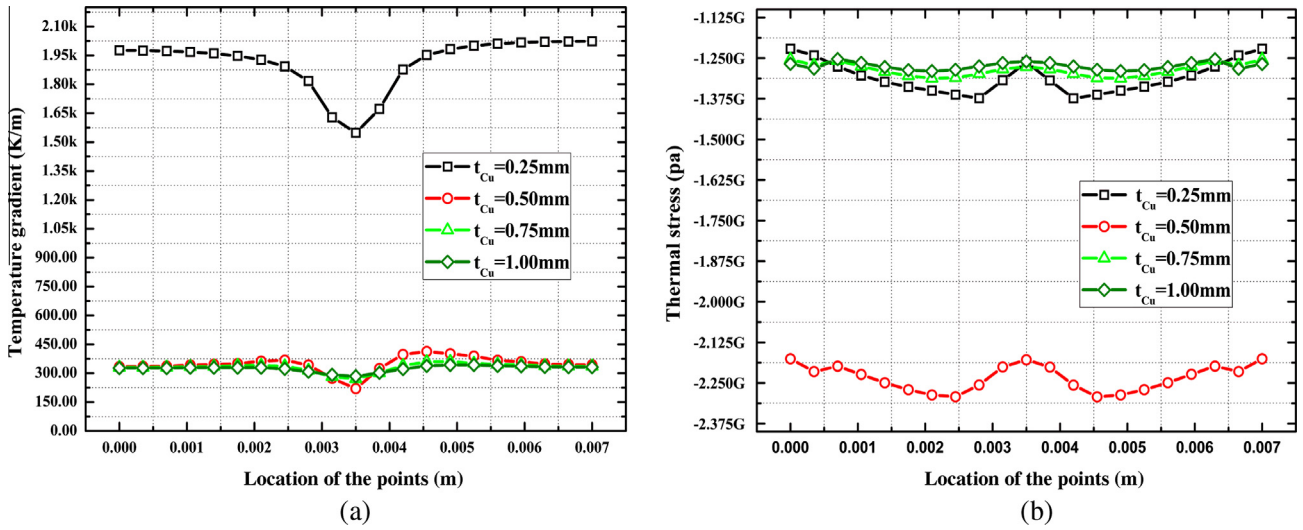


Fig. 14. The influence of copper conducting strip thickness on the thermoelectric module (Line 3): (a) distribution of temperature gradient and (b) distribution of  $\sigma_1$ .

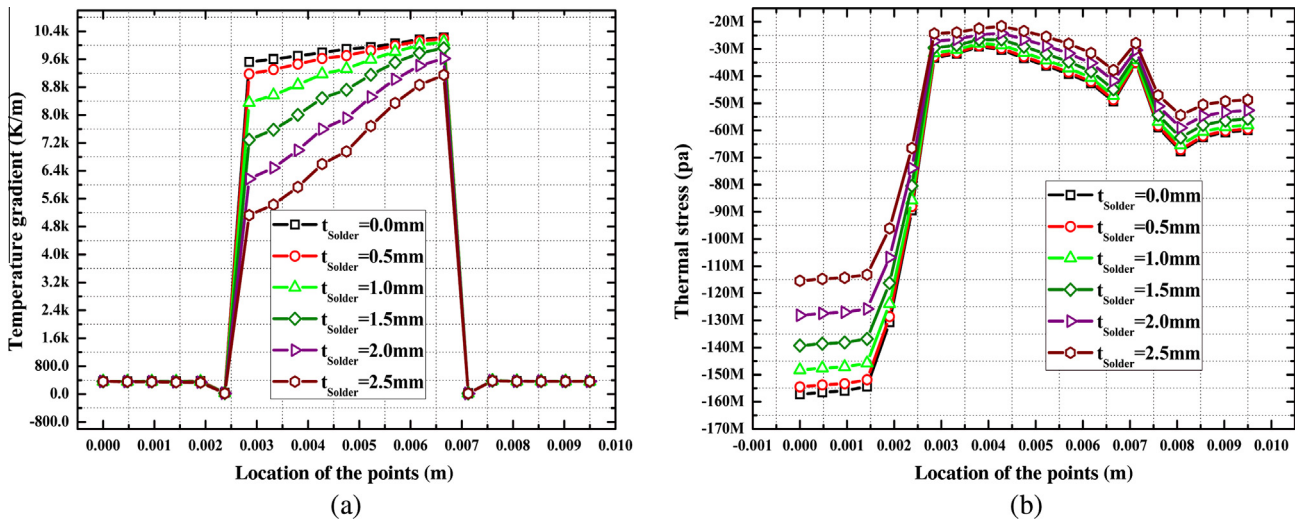


Fig. 15. The influence of tin soldering thickness on the thermoelectric module (Line 1): (a) distribution of temperature gradient and (b) distribution of  $\sigma_1$ .

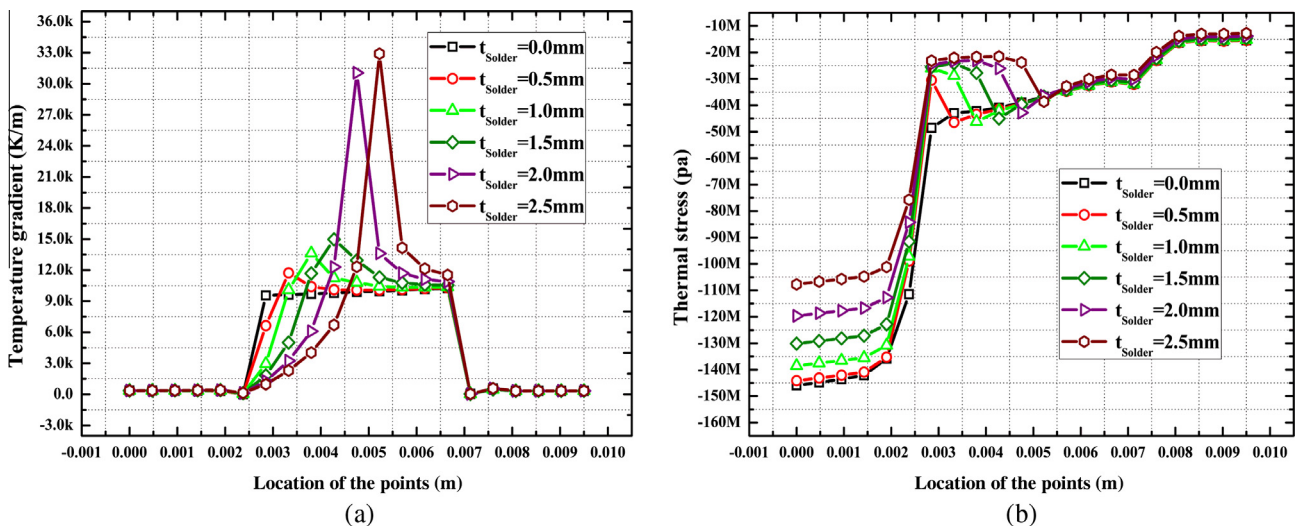


Fig. 16. The influence of tin soldering thickness on the thermoelectric module (Line 2): (a) distribution of temperature gradient and (b) distribution of  $\sigma_1$ .

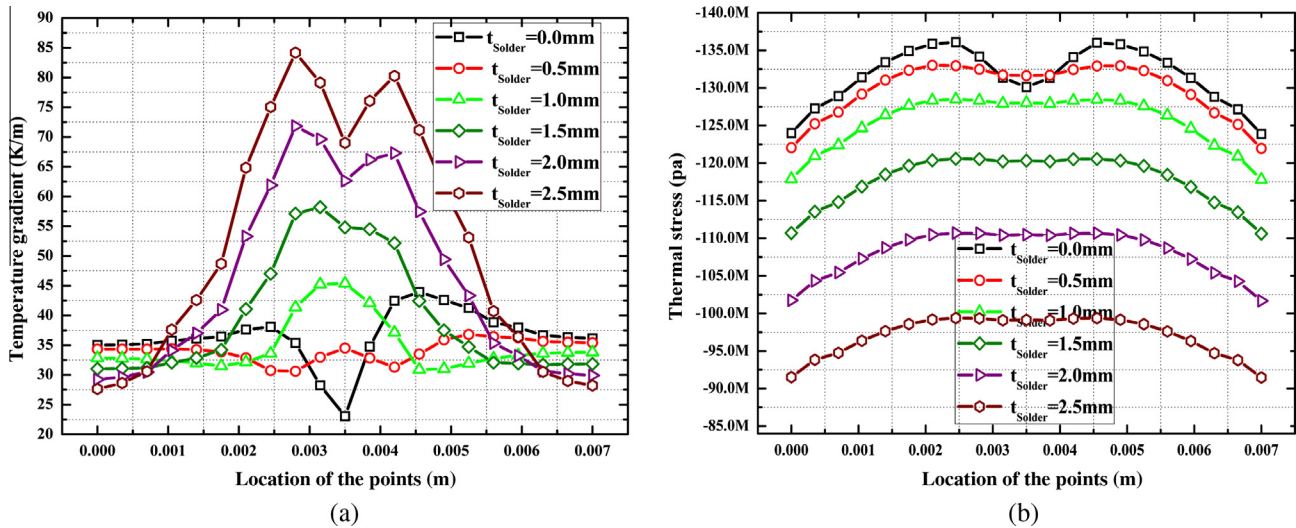


Fig. 17. The influence of tin soldering thickness on the thermoelectric module (Line 3): (a) distribution of temperature gradient and (b) distribution of  $\sigma_1$ .

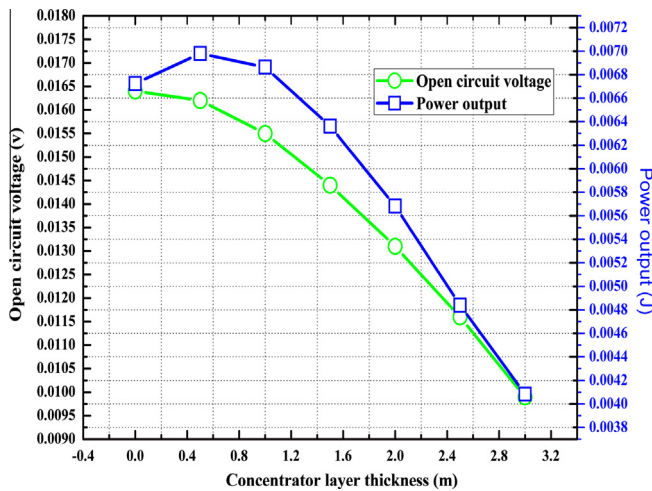


Fig. 18. Open circuit voltage and maximum power output of thermoelectric modules for various tin soldering thickness.

a benefit to the design and application of thermoelectric generators/refrigerators and/or photovoltaic panels being imposed on high heat flux to achieve higher energy transfer efficiency.

#### 4. Conclusion

Thermodynamic and thermal stress analysis of a thermoelectric generator is carried out for different module geometry configurations. All the results are examined by different heat flux boundary conditions on the same order of magnitude which demonstrates that the conclusions are valid. It is found that:

- (1) A larger ceramic plate thickness ( $\geq 2.5$  mm) is effective to alleviate thermal stress and protect the device at the same time. In the condition that the total heat flow is constant, the influence of ceramic plate thickness on efficiency, power and open circuit voltage output is negligible.
- (2) A smaller distance between thermo-pins helps to restrain thermal stress development and to prolong the lifecycle of the thermoelectric module.
- (3) Either a thicker ( $\geq 0.50$  mm) or thinner ( $\leq 0.50$  mm) copper conducting strip effectively reduces thermal stress. To save copper material, a smaller thickness proves a better choice.

- (4) To prolong the lifecycle of a thermoelectric generator module, tin soldering is applied to improve the temperature distribution in the module. Choosing a suitable tin soldering thickness will not only alleviate thermal stress intensity in the module, but also increase thermal efficiency.

#### Acknowledgements

This research was supported by the National Natural Science Foundation of China (51106060) and the Natural Science Foundation of Hubei Province China (2012FFB02214).

#### References

- [1] Sahin AZ, Yilbas BS. The thermoelement as thermoelectric power generator: effect of leg geometry on the efficiency and power generation. *Energy Convers Manage* 2013;65:26–32.
- [2] Khattab NM, Shenawy ETE. Optimal operation of thermoelectric cooler driven by solar thermoelectric generator. *Energy Convers Manage* 2006;47:407–26.
- [3] Merbati ASA, Yilbas BS, Sahin AZ. Thermodynamics and thermal stress analysis of thermoelectric power generator: influence of pin geometry on device performance. *Appl Therm Eng* 2013;50:683–92.
- [4] Rodríguez A, Vián JG, Astrain D, Martínez A. Study of thermoelectric systems applied to electric power generation. *Energy Convers Manage* 2009;50:1236–43.
- [5] O'Brien RC, Ambrosi RM, Bannister NP, Howe SD, Atkinson HV. Safe radioisotope thermoelectric generators and heat sources for space applications. *J Nucl Mater* 2008;377:506–21.
- [6] Yilbas BS, Sahin AZ. Thermoelectric device and optimum external load parameter and slenderness ratio. *Energy* 2010;35:5380–4.
- [7] Omer SA, Infield DG. Design and thermal analysis of a two stage solar concentrator for combined heat and thermoelectric power generation. *Energy Convers Manage* 2000;41:737–56.
- [8] Maneewan S, Hirunlabh J, Khedari J, Zeghamati B, Teekasap S. Heat gain reduction by means of thermoelectric roof solar collector. *Sol Energy* 2005;78:495–503.
- [9] Zhou S, Sammakia BG, White B, Borgesen P. Multiscale modeling of thermoelectric generators for the optimized conversion performance. *Int J Heat Mass Transf* 2013;62:435–44.
- [10] Xiao J, Yang T, Lib P, Zhai P, Zhang Q. Thermal design and management for performance optimization of solar thermoelectric generator. *Appl Energy* 2012;93:33–8.
- [11] Whalen SA, Applett CA, Aselage TL. Improving power density and efficiency of miniature radioisotopic thermoelectric generators. *Orig Res Article J Power Sources* 2008;50:657–63.
- [12] Chein R, Chen Y. Performances of thermoelectric cooler integrated with microchannel heat sinks. *Int J Refrig* 2005;28:828–39.
- [13] Astrain D, Vián JG, Martínez A, Rodríguez A. Study of the influence of heat exchangers' thermal resistances on a thermoelectric generation system. *Energy* 2010;35:602–10.

- [14] Zhang Q, Agbossou A, Feng Z, Cosnier M. Solar micro-energy harvesting based on thermoelectric and latent heat effects Part II: experimental analysis. *Sensors Actuat A* 2010;163:284–90.
- [15] Agbossou A, Zhang Q, Sebald G, Guyomar D. Solar micro-energy harvesting based on thermoelectric and latent heat effects Part I: theoretical analysis. *Sensors Actuat A* 2010;163:277–83.
- [16] Zhao Z, Yang T, Xia S. Entropy and heat efficiency analysis of solar thermoelectric generator device. *China Water Transp* 2007;1(5):185–7.
- [17] Huang M, Yen R, Wang A. The influence of the Thomson effect on the performance of a thermoelectric cooler. *Int J Heat Mass Transf* 2005;48:413–6.
- [18] Freunek M, Miller M, Urgan T, Walker W, Reindl L. New physical model for thermoelectric generators. *J Electron Mater* 2009;38:1214–20.
- [19] Wahab SAA, Elkamel A, Damkhi AMA, Habsi IAA, Rubai'ey' HSA, Battashi AKA, et al. Design and experimental investigation of portable solar thermoelectric refrigerator. *Renew Energy* 2009;34:30–4.
- [20] Omer SA, Infield DG. Design optimization of thermoelectric devices for solar power generation. *Sol Energy Mater Sol Cells* 1998;53:67–82.
- [21] Vián JG, Astrain D. Development of a heat exchanger for the cold side of a thermoelectric module. *Appl Therm Eng* 2008;28:1514–21.
- [22] Hsiao YY, Chang WC, Chen SL. A mathematic model of thermoelectric module with applications on waste heat recovery from automobile engine. *Energy* 2010;35:1447–54.
- [23] Gou X, Xiao H, Yang S. Modeling, experimental study and optimization on low-temperature waste heat thermoelectric generator system. *Appl Energy* 2010;87:3131–6.
- [24] Hsu C, Huang G, Chu H, Yud B, Yao D. Experiments and simulations on low-temperature waste heat harvesting system by thermoelectric power generators. *Appl Energy* 2011;88:1291–7.
- [25] Lertsatitthanakorn C, Khasee N, Atthajariyakul S, Soponronnarit S, Therdyothin A, Suzuki RO. Performance analysis of a double-pass thermoelectric solar air collector. *Sol Energy Mater Sol Cells* 2008;92:1105–9.
- [26] Rowe DM. *Thermoelectrics handbook*. Boca Raton: CRC Press; 2006.